Quantum Scattering in a Juggling Atomic Fountain

Ronald Legere and Kurt Gibble

Department of Physics, Yale University, New Haven, Connecticut 06520-8120

(Received 19 August 1998)

We demonstrate a juggling atomic fountain by launching two laser-cooled balls of ^{133}Cs atoms in rapid succession. The atoms collide near the top of the fountain and, by varying the delay between launches, we scan the collision energy from 19 to 150 μK. We measure the differential scattering cross section and isolate the contributions from different partial waves including their interferences. We observe the s-wave energy dependence and the p-wave scattering threshold. We infer a triplet s-wave scattering length of $-400a_0$ and a p wave of $(-107a_0)^3$ for $|F = 4, m = 4\rangle + |3, 3\rangle$. [S0031-9007(98)08031-4]

PACS numbers: 34.50.–s, 06.30.Ft, 32.80.Pj

Many interesting effects of low energy quantum scattering have been beautifully demonstrated in electron-atom scattering [1] and in nuclear physics [2]. Here, we observe for the first time the scattering of multiple atomic partial waves, the interference between them, and the p-wave quantum scattering threshold. Low energy atomic scattering is currently important in many areas of modern atomic physics including Bose-Einstein condensation (BEC) [3], atom interferometers [4], and atomic clocks [5].

Low energy atomic collisions have previously been observed in a variety of experiments. The first observations studied cryogenically cooled H [6] and later He [7] gases. More recently, cold collisions have played the crucial role of thermalizing dilute gases in magnetic traps [3,8–10] during evaporative cooling to achieve BEC. In addition, inelastic cold collisions can inhibit the cooling to the BEC transition [11]. Another important and harmful effect of collisions is the large frequency shift they produce in laser-cooled clocks [5]. Finally, photoassociation spectroscopy [10,12] has provided detailed information to characterize cold collisions [13].

All of the above experiments are largely insensitive to the angular distribution of the scattered atoms. Previously, we observed the angular distribution of Cs-Cs collisions and showed that collisions are 99.9(1)% s wave at 0.89 μK [14]. Here, we demonstrate a new technique, a juggling atomic fountain, where we scatter Cs atoms off of one another with a well-defined collision energy. We vary the collision energy from low energies, where the scattering is s wave, since the de Broglie wavelength is much longer than the scale of the interatomic potential [15], up to energies at which several partial waves are allowed.

We *juggle* atoms by launching two balls of laser-cooled atoms with a short time delay Δt. The two balls are launched vertically at the same velocity and collide near the top of the fountain with a relative velocity $v_r = \Delta t \times g$, where $g = 9.8$ m/s^2. Launch delays of $\Delta t = 7$ to 20 ms correspond to collision energies of $E_c/k_B = mg^2\Delta t^2/4k_B = 19$ to 150 μK. We prepare each ball in a particular $|F, m\rangle$ state using optical pumping and a two-photon Raman transition [16]. After the atoms scatter, another two-photon Raman transition is used to detect the vertical velocity component, thereby measuring the angular distribution of the scattering. This is a complete scattering experiment: state-to-state velocity-selected differential crossed-beam scattering at μK energies.

Our juggling fountain is based on a double magneto-optical trap (MOT) (see Fig. 1) [14]. The vapor cell MOT has a lifetime of 0.1 s and repeatedly loads the UHV MOT. We use ten launches to load 5×10^9 Cs atoms. To juggle, we launch two balls from the UHV MOT. For this, we hold the repeatedly loaded (1st) ball in the UHV MOT while loading the vapor cell MOT with a 2nd ball. The 2nd ball is then launched and, shortly before it reaches the UHV MOT, the 1st ball is launched upward. We then capture the 2nd ball in the UHV MOT, trap it for as little as 1 ms, and then launch it. The launch duration is 2.5 ms, the velocity typically is 1.85 m/s, and T = 1.5 μK.

The trapping and cooling light for the 2nd ball perturbs the 1st ball for short launch delays. For a 7 ms delay, the 1st ball is only $\approx$1 cm above the trap when the 2nd ball is trapped. Since the diameter of each ball is 1.2 cm, we must protect the 1st ball from the trapping light. We protect the atoms by (1) hiding the 1st ball

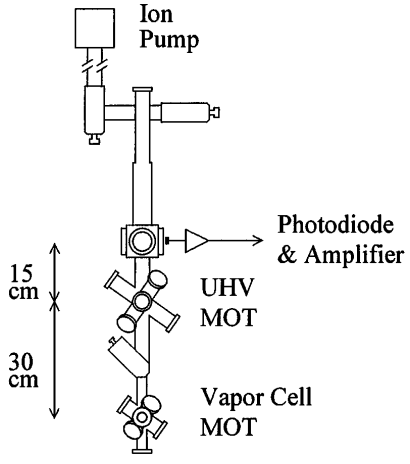

FIG. 1. The double MOT fountain.

 0031-9007/98/81(26)/5780(4)$15.00

by hyperfine pumping the atoms into the $6S\ F = 3$ state with light tuned to the $6S_{1/2}\ F = 4 \rightarrow 6P_{3/2}\ F' = 4'$ transition, (2) masking the top of the trapping beams to minimize the trapping light on the 1st ball, and (3) attenuating and carefully aiming the repumping light to prevent repumping the 1st ball. For the shortest (long) delays, at least 50% (90%) of the atoms in the 1st ball survive the launch of the 2nd ball.

Each ball is prepared in a particular $|F, m\rangle$ state. Here, we collide $6S\ |3,3\rangle$ and $6S\ |4,4\rangle$ atoms. First, we optically pump both balls into $6S\ |4,4\rangle$. To minimize the heating during pumping, we use simultaneous 2 ms pulses of circularly polarized light tuned to $6S_{1/2}\ F = 4 \rightarrow 6P_{3/2}\ F' = 4'$ and $F = 3 \rightarrow 3'$. Since the $|3,3\rangle$ state is also a dark state for this light, we repump these atoms with a 0.3 ms pulse of light tuned to $F = 3 \rightarrow 4'$. To get 90% of the atoms into the $|4,4\rangle$ state, we repeat this sequence (for each ball) and measure [14] a final temperature of $3-3.5\ \mu$K along the axis of the pumping beams. During this phase, we pulse a 0.8 G magnetic field into the plane of Fig. 1, along the circularly polarized laser beams.

We transfer the 2nd ball from the $|4,4\rangle$ state to the $|3,3\rangle$ state using a velocity-selective two-photon Raman transition [17]. This *selection* has a Blackman intensity profile [14] insuring that there are essentially no atoms in the wings of the $|3,3\rangle$ state velocity distribution. The Raman beams, from two phase-locked lasers, are detuned 3 GHz from the $6P_{3/2}$ transition, have crossed linear polarization, and propagate out of the plane of Fig. 1. To drive the transition, we switch the bias field to a vertical field of 0.8 G. The selection efficiency is $>80\%$ and depends on the probe bandwidth discussed below. Typically the 2nd ball has $\frac{1}{4}$ the atoms of the 1st.

After the two balls collide we *probe* the velocity distribution of the $|3,3\rangle$ state by driving a velocity-selective two-photon Raman transition to the $|4,4\rangle$ state. We then measure the $F = 4$ population using light tuned to $F = 4 \rightarrow 5'$, detecting the fluorescence with a 1 cm^2 photodiode. However, first we must clear the $F = 4$ atoms in the 1st ball. We *clear* these atoms 15 ms before the two-photon Raman probe by irradiating the atoms with a pulse of circularly polarized light tuned to $F = 4 \rightarrow 5'$.

We adjust the velocity bandwidth of the probe by controlling the angle between the Raman beams. To probe the vertical velocity component, $\mathbf{k}_1 - \mathbf{k}_2$ is vertical, where $\mathbf{k}_1$ and $\mathbf{k}_2$ are the Raman beams' wave vectors. The velocity width is $\Delta v_z = \pi \Delta\nu / [k_1 \sin(\theta/2)]$ where $\Delta\nu = 1.3$ kHz is the Raman $1/e$ half-width, θ is the angle between $\mathbf{k}_1$ and $\mathbf{k}_2$, and $k_1 \approx k_2$. Typically, $\theta \approx 6°$; larger θ implies more resolution but fewer detected atoms (less signal to noise). We choose $\Delta v_z \approx v_r/10$ so we can distinguish the various partial waves.

In Fig. 2 we show scans of the Raman probe frequency over the velocity distributions for $\Delta t = 12$ ms. In addition to the "collisions" data [solid curves in Figs. 2a-(i) and 2a-(ii)], we take several backgrounds to remove systematic effects [14]. First, we measure the uncollided velocity distribution of the 2nd ball by clearing the 1st ball 5 ms after we select the 2nd ball yielding the "no-collisions" signal [dashed curves in Figs. 2a-(i) and 2a-(ii)]. For both the "collisions" and "no-collisions" data, there is a significant background due to the off-resonant excitation of $F = 4$ atoms during the clearing and selection pulses. We measure this by detuning the selection pulse [Fig. 2a-(iii)] and then subtract these from the raw "collisions" and "no-collisions" signals to obtain the curves Figs. 2a-(i) and 2a-(ii). Therefore, four launches are required to measure the number of scattered atoms at each velocity—early and late clearing combined with selection and no selection. We also measure the baseline offset by detuning the Raman probe.

In Fig. 2b, the velocity distribution of the scattered atoms is the difference between the "collisions" and "no-collisions" signals. Since this difference is much smaller than the peak background level [Fig. 2a-(iii)], we have studied these backgrounds [18]. When we change the detuning, location, and pulse length of the clearing beam, the background levels change but the scattering signal is unchanged. In addition, we collect data as in Fig. 2b except we drop the 2nd ball instead of launching it to verify that the clearing and Raman beams and the launching do not mimic scattering. We also reduce the density of the 1st ball and see no scattering. Finally, to ensure that the clearing beam does not perturb the 2nd

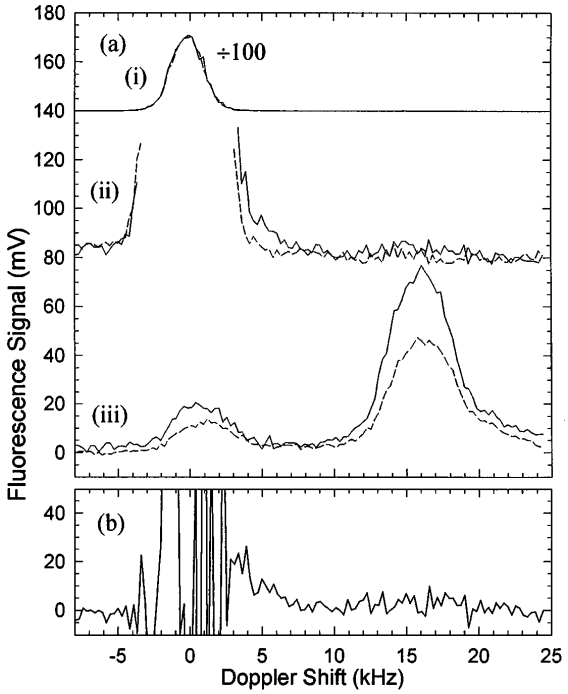

FIG. 2. (a) Measured velocity distributions for a 12 ms launch delay. Data with late (early) clearing are shown with solid (dashed) lines. We show the "collisions" (late clearing) and "no-collisions" (early clearing) signals reduced by 100 (i) and full size (ii) where the backgrounds (iii) have been subtracted. (b) The effect of scattering is "collisions" − "no-collisions." Here, $\approx 0.7\%$ of the selected atoms scatter.

ball, we insert an additional clearing pulse for each scan, just after the time of the early clearing pulse.

In Fig. 3 we show the scattering for launch delays $\Delta t = 7-20$ ms where the noisy central region is omitted for clarity. The solid (dashed) curves are the measured (calculated) velocity distributions. For the calculations, we start with a differential cross section:

$$\frac{d\sigma}{d\Omega} = \frac{1}{k^2}\left|\sum_\ell (2\ell + 1)e^{i\delta_\ell}\sin\delta_\ell P_\ell(\cos\theta)\right|^2 = \frac{1}{k^2}(\sin^2\delta_0 + 6\sin\delta_0\sin\delta_1\cos(\delta_0 - \delta_1)\cos\theta + 9\sin^2\delta_1\cos^2\theta + \ldots), \quad (1)$$

where $k = mv_r/2\hbar$, δ_ℓ is the phase shift of the ℓth partial wave, $\sigma_\ell = 4\pi/k^2\ (2\ell + 1)\sin^2\delta_\ell$, P_ℓ is a Legendre polynomial, and θ is the center-of-mass scattering angle. This is averaged over the three dimensional velocity distributions of each ball [19] and convolved with the probe response. We include s, p, and d waves.

While the total cross section is just the sum of the partial cross sections σ_ℓ, the angular distribution of the scattering is very sensitive to the quantum interferences between partial waves. Because the $\cos\theta$ interference term in Eq. (1) is proportional to $\sqrt{\sigma_1}$ for $\delta_1 \ll 1$, the velocity distributions in Fig. 3 are sensitive to small partial cross sections, and especially the relative signs of the phase shifts δ_ℓ. For example, for $\Delta t = 9$ ms, σ_1/σ is only 0.21 but has a large effect on the resulting differential cross section. This is shown in Fig. 3 as the dotted curve is pure s-wave scattering and, for the dot-dashed, $\delta_1/\delta_0 < 0$. It is clear that δ_0 and δ_1 have the same sign since the scattering interferes constructively in the forward direction. For the calculations, the magnitude of the s-p interference depends on the relative phase shift $\delta_0 - \delta_1$. However, for this range of energies, we find $\cos(\delta_0 - \delta_1) > 0.8$ and therefore we see nearly maximal interference of the s and p (and also d) waves.

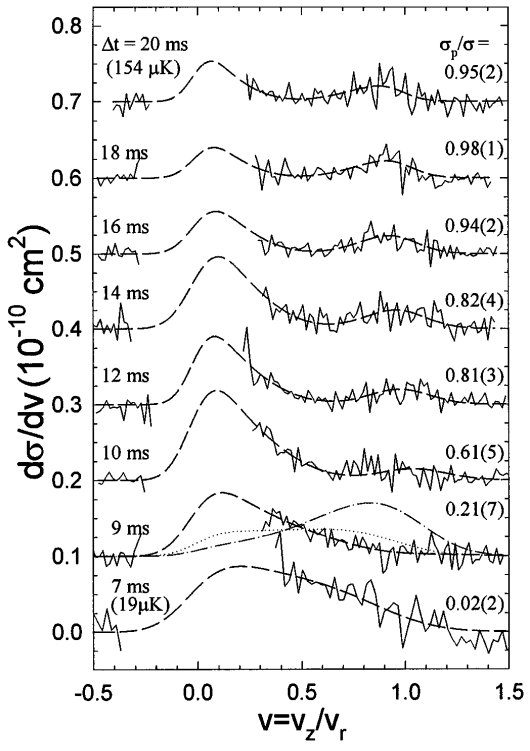

FIG. 3. Velocity distributions for launch delays from 7 to 20 ms. The dashed lines are calculations using the indicated p-wave fractions. For 9 ms, the dotted line is pure s-wave, and the dot-dashed line is for $\delta_1/\delta_0 < 0$.

To obtain differential cross sections, we measure the density at each collision energy using laser absorption, optical pumping, and the saturation of fluorescence [20]. We measure the $1/e$ radius of each ball to be typically 0.6 cm just after the optical pumping and the peak density of the 1st ball to be $1.0(7) \times 10^9$ cm^{-3}. We measure the size and temperature along each axis of each ball using Raman spectroscopy, time-of-flight techniques, and fluorescence imaging. To calculate a cross section, we integrate the product of the density distributions of the two balls over the time between the early and late clearing pulses [21]. We take the density and velocity distributions of each ball to be Gaussians. For the fountain heights we use, the two balls overlap when the 1st ball is cleared, but the number of scattered atoms is $>80\%$ of the number that would scatter if the two balls passed entirely through each other. With a taller fountain, more atoms would scatter but then more of the scattered atoms would leave the detection region. Thus, for long launch delays, we use a shorter fountain so that the two balls have nearly the same separation at the detection region. Just after the two balls collide, the scattered atoms form a spherical shell where the diameter of the shell is the same as the separation between the two balls and the radial thickness of the shell is approximately the diameter of the balls. The size of the detection region is limited by the 2.4 cm diameter Raman laser beams. The typical separation between the balls was 0.7 cm when detected and, for the longest delay, 1.0 cm. In this way, detection effects are largely eliminated, but there may still be some biases at the highest energies.

For juggling, the distribution of collision energies is much narrower than in a thermal sample. Nonetheless, we account for the distribution of collision energies for each launch delay. We begin with a threshold energy dependence for each partial cross section. This yields partial cross sections at each E_c similar to the data in Fig. 4. We then refit using the "measured" energy dependence

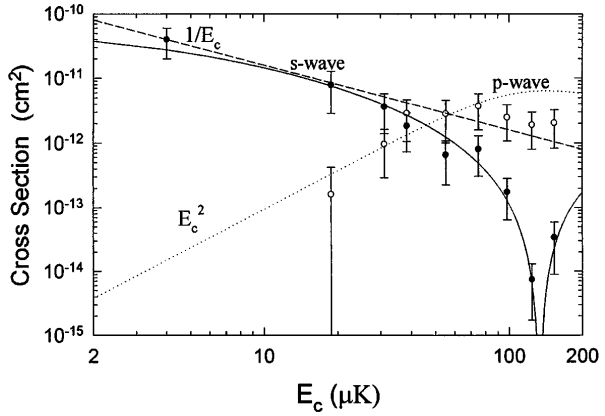

FIG. 4. Energy dependence of s-wave (filled) and p-wave (open) scattering for $|F = 4, m_F = 4\rangle + |3, 3\rangle$. We show a $1/E_c$ energy dependence (dashed line), the s-wave energy dependence for a square well (solid line), and the p-wave scattering for $a_1 = (-107a_0)^3$ (dotted line).

to calculate velocity distributions. Because of the narrow distribution of collision energies, this procedure converges in one iteration. In Fig. 4, we plot a point for each $E_c = mg^2\Delta t^2/4$ where we determine the cross section at E_c using the measured energy dependence [22].

The s-wave cross section in Fig. 4 rises as $1/E_c$ for $E_c < 30\ \mu$K. The s-wave interaction is pure triplet for $|4, 4\rangle + |3, 3\rangle$. Since the unitary limit ($4\pi/k^2$) is three times higher, we do not see a zero energy triplet resonance [9]. A detailed analysis suggests that the $1/E_c$ dependence occurs because there is a region of constant δ_0 and the scattering length $a_{\ell=0} \approx -400a_0$ [23]. Whenever $a_\ell < 0$, there must be a region of constant phase since δ_ℓ must decrease [15] at high energy. The Ramsauer-Townsend minimum [1] near 150 μK also points to $a_{\ell=0} < 0$ as this is a relatively low energy. For reference in Fig. 4, we also show the s-wave cross section for a deep square well (solid line) using $a_{\ell=0} \approx -400a_0$ and a range of $137a_0$. The scattering length is consistent with one recent analysis and differs slightly from another [24].

In Fig. 4, the low-energy p-wave cross sections follow the quantum scattering threshold $\sigma_1 = 12\pi a^2 k^4 \propto E^2$ since $\tan(\delta_\ell) \approx -a_\ell k^{2\ell+1}$ for $k \to 0$ [15]. The dotted curve in Fig. 4 corresponds to $a_1 = [-107(6)a_0]^3$. The p-wave scattering length is negative since $a_{\ell=0} < 0$ and the s-p interference shows δ_0 and δ_1 have the same sign. At higher energies, the p wave departs from threshold behavior, decreasing before reaching the unitary limit (5 times higher) as expected for $a_1 < 0$. Since the p-wave channel for $|4, 4\rangle + |3, 3\rangle$ is an admixture of singlet and triplet, these measurements will further refine the potentials [24]. For d waves, the best fit indicates $a_2 = [-52(7)a_0]^5$ although there may be a systematic error for high energies where the d waves contribute most.

Finally, we note that juggling is important for future atomic clocks. Typically fountain clocks have interrogation times of 0.5 s and a launch rate of 1 s^{-1}. Launching atoms every 30 ms improves the short-term stability and reduces the local oscillator requirements by eliminating the dead time [25]. In a juggling fountain clock, the frequency shift due to collisions between successive balls will be important. The energy dependences in Fig. 4 suggest there will be optimal juggling rates.

We acknowledge discussions with Servaas Kokkelmans and Boudewijn Verhaar, and financial support from the NSF and a NIST Precision Measurement Grant.

[1] C. Ramsauer, Ann. Phys. (Leipzig) **72**, 345 (1923); J. S. Townsend and V. A. Bailey, Philos. Mag. **43**, 593 (1922); H. S. W. Massey, *Atomic and Molecular Collisions* (Taylor and Francis, London, 1979).
[2] J. M. Blatt and V. F. Weisskopf, *Theoretical Nuclear Physics* (John Wiley & Sons, New York, 1952).
[3] W. Ketterle and N. J. Van Druten, Adv. At. Mol. Opt. Phys. **37**, 181 (1996).
[4] *Atom Interferometry*, edited by P. R. Berman (Academic Press, San Diego, 1997).
[5] K. Gibble and S. Chu, Phys. Rev. Lett. **70**, 1771 (1993).
[6] See M. E. Hayden and W. N. Hardy, Phys. Rev. Lett. **76**, 2041 (1996).
[7] J. C. Mester *et al.*, Phys. Rev. Lett. **71**, 1343 (1993).
[8] N. Masuhara *et al.*, Phys. Rev. Lett. **61**, 935 (1988).
[9] M. Arndt *et al.*, Phys. Rev. Lett. **79**, 625 (1997).
[10] D. J. Heinzen, Int. J. Mod. Phys. B **28**, 3297 (1997).
[11] J. Söding *et al.*, Phys. Rev. Lett. **80**, 1869 (1998).
[12] A. Fioretti *et al.*, Phys. Rev. Lett. **80**, 4402 (1998).
[13] J. M. Vogels *et al.*, Phys. Rev. A **56**, R1067 (1997); S. J. J. M. F. Kokkelmans *et al.*, *ibid.* **56**, 4389 (1997).
[14] K. Gibble, S. Chang, and R. Legere, Phys. Rev. Lett. **75**, 2666 (1995).
[15] J. R. Taylor, *Scattering Theory* (Wiley, New York, 1972).
[16] M. Kasevich *et al.*, Phys. Rev. Lett. **66**, 2297 (1991).
[17] We control the five independent 1st derivatives of the magnetic field. The inhomogeneous width is 800 Hz.
[18] The backgrounds do not depend on Δt. Excluding velocities where the background is larger than the scattering does not change the fits. (An anomalously large "collisions" background yields a negative scattering signal.)
[19] The thermal velocities for the collision kernel are anisotropic from the state preparation. See P. F. Liao, J. E. Bjorkholm, and P. R. Berman, Phys. Rev. A **21**, 1927 (1980).
[20] K. E. Gibble, S. Kasapi, and S. Chu, Opt. Lett. **17**, 526 (1992).
[21] We neglect the correlation between position and velocity [14] since the optical pumping adds much of the temperature right before the collisions and $E_c \gg T$.
[22] For $E_c = 4\ \mu$K, we probe $|4, 4\rangle + |3, 3\rangle$ collisions in one ball [14] and use this to monitor the density for juggling.
[23] S. Kokkelmans (private communication).
[24] S. Kokkelmans, B. J. Verhaar, and K. Gibble, Phys. Rev. Lett. **81**, 951 (1998); P. J. Leo *et al.*, *ibid.* **81**, 1389 (1998).
[25] K. Gibble, in *Proceedings of the Fifth Symposium on Frequency Standards and Metrology*, edited by J. C. Bergquist (World Scientific, Singapore, 1996), p. 66.